



Roles of reactive species in photocatalysis: effect of scavengers and inorganic ions on dye removal from wastewater

A. Ahmadian¹ · S. Ahmadi² · B. A. Goharrizi¹

Received: 12 September 2022 / Revised: 24 January 2023 / Accepted: 16 March 2023 / Published online: 24 April 2023

© The Author(s) under exclusive licence to Iranian Society of Environmentalists (IRSEN) and Science and Research Branch, Islamic Azad University 2023

Abstract

Photocatalytic degradation is an effective technique for removing dyes from contaminated water. Herein, a nanocomposite that contains banana peel activated carbon and nanoparticles of zinc oxide (BPAC/ZnO) was prepared by the physical mixing method. The impact of inorganic anions (Cl^- , HCO_3^- , NO_3^- , and F^-) and cations (Al^{3+} and Ca^{2+}) at different concentrations (2, 10, 30 mM) was examined. This work investigates the incorporation of ZnO nanoparticles onto activated carbon in order to enhance the photocatalytic degradation of Acid Blue 25 (AB25). Under the optimum conditions of effective parameters, the effect of different scavengers (EDTA, ethanol, KI, NaN_3 , $\text{Na}_2\text{S}_2\text{O}_8$, NaBrO_3 , H_2O_2 , and BQ) at various concentrations (2, 10, and 30 mM) was investigated. The results showed that h^+ and $\text{O}_2^{\cdot-}$ play a pivotal role in the Acid Blue 25 removal. Also, it should be noted that hydroxyl radicals play a supplementary role in the photocatalytic degradation of Acid Blue 25. Also, electron scavengers, including $\text{Na}_2\text{S}_2\text{O}_8$ and NaBrO_3 , increased the degradation rate. Among the anions, NO_3^- exhibited the strongest inhibition potential. Inorganic anions inhibited the photocatalytic removal of AB25 in the following order $\text{NO}_3^- \geq \text{F}^- \geq \text{HCO}_3^- \geq \text{Cl}^-$. Likewise, Al^{3+} showed the highest inhibition among cations.

Editorial responsibility: Hari Pant.

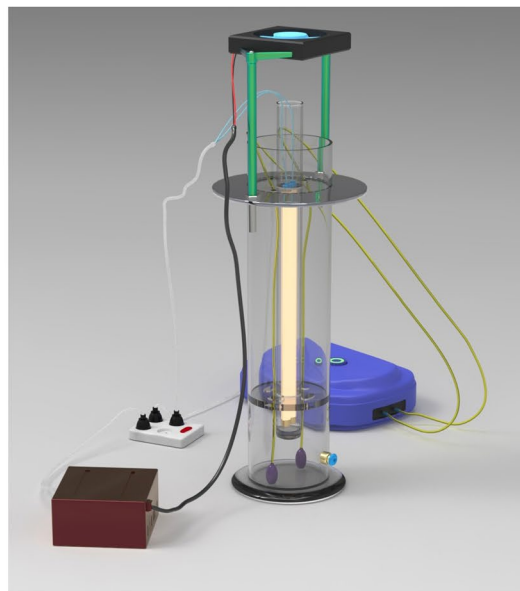
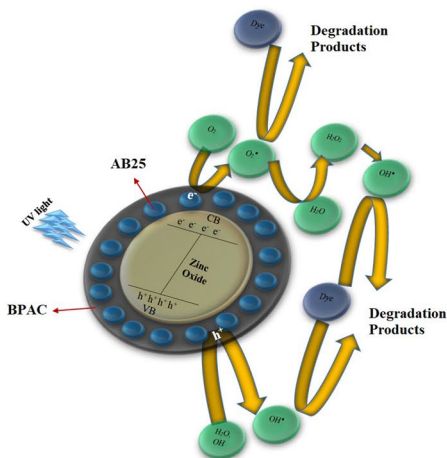
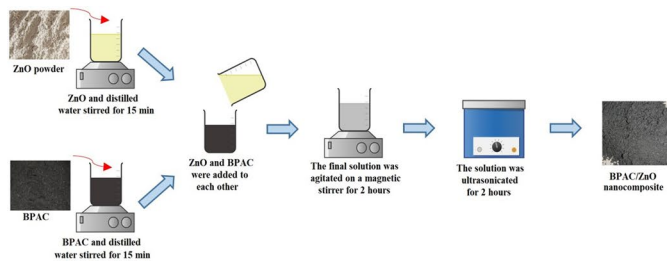
✉ B. A. Goharrizi
bamin@ut.ac.ir

¹ Faculty of Environment, University of Tehran,
Tehran 14155-6619, Iran

² Environmental and Chemical Engineering Research Unit,
Faculty of Technology, University of Oulu, 90014 Oulu,
Finland



Graphic abstract



Keywords Inorganic ions · Scavengers' study · Photocatalysis · Inhibition effect · Superoxide radicals

Introduction

Dyes are used in some industries such as textiles, paper, and plastics. Numerous industries discharge a substantial amount of wastewater into the aquatic environment. As a result, the life of plants, humans, and animals are under threat (Chhabra et al. 2020; Picos-Benítez et al. 2020; Shfieizadeh et al. 2022). The annual production amount of dyes is estimated to be approximately 700,000 tons, 15% of which is wasted during industrial processes (Azzam et al. 2019; Singh et al. 2019; Samsami et al. 2020). The discharge of synthetic dyes into the environment may lead them to be very persistent and contributes to serious health problems (Brindha et al. 2022). Also, the presence of dyes in waterbodies would reduce light penetration and could be a major obstacle to photosynthesis (Yoon et al. 2012). Anthraquinone dyes such as Acid Blue 25 (AB25) are used in various industries. This chemical compound has complex structures as well as high molecular weight resulting in a time-consuming breakdown of its bonds (Daneshvar et al. 2014).

Dye removal from wastewater can be accomplished by using several methods, such as adsorption, electrocoagulation, and advanced oxidation processes (Ahmadian et al.

2022). Advanced oxidation processes (AOPs) have proven to be one of the most effective ways to remove a variety of organic contaminants from wastewater. (Babaei et al. 2021; Guan et al. 2021). Among AOPs, photocatalysis is considered to be a sustainable and greener method for degrading organic pollutants (Wang et al. 2020; Chen et al. 2021b; Nippes et al. 2022). Several types of semiconductors, such as zinc oxide (ZnO), are widely used in photocatalytic reactions due to their high stability and low cost (Sakarkar et al. 2020; Sidik et al. 2020; Moawed et al. 2022). One of the best ways to improve photocatalytic efficiency is to increase the interaction between pollutants and photocatalysts. The mass transfer of contaminants onto catalyst surfaces can be enhanced by using materials such as activated carbon.

Pollutant degradation by photocatalysis occurs when a pollutant reacts with oxidizing species, some examples of which are hydroxyl radicals ($\cdot\text{OH}$), valence band holes ($h\nu^+$), and superoxide radicals ($\text{O}_2^{\cdot-}$) (Palominos et al. 2008; Daimon et al. 2008; Li et al. 2011). The contributions of each oxidizing species in photocatalytic degradation depend heavily on the nature of the contaminant (Makama et al. 2020). Consequently, the identification of the oxidant, which is responsible for oxidizing the pollutant, is vital. In order to maximize



efficiency, it is essential to pinpoint the precise role played by each oxidizing species in photocatalysis and understand how pollutant degradation occurs.

There are many inorganic ions in natural water and wastewater, including Cl^- , HCO_3^- , NO_3^- , SO_4^- , and F^- as anions and K^+ , Na^+ , Ca^{2+} , and Mg^{2+} as cations (Wang et al. 2012; Zelmanov and Semiat 2015). A considerable amount of inorganic salts can be found in textile industries' wastewater (Guillard et al. 2003; Chen et al. 2021a). The presence of inorganic ions in wastewater can affect the removal of contaminants (Santiago et al. 2014; Tang et al. 2018). As an example, Cl^- is an inorganic ion frequently used in textile dyeing as a promoter (Huang et al. 2018; Chen et al. 2021a).

This work aims to evaluate the effect of reactive species (hydroxyl radical ($\text{OH}\cdot$), holes (h^+), electron (e^-), and superoxide radical ($\text{O}_2\cdot^-$)) and the impact of inorganic anions and cations on the photocatalytic degradation of AB25 in order to provide better insight of the mechanism. To the best of our knowledge, no research has been conducted to examine the effect of reactive species and inorganic ions on the photocatalytic degradation of AB25. The results of this work may provide helpful guidance for other photocatalytic applications.

Materials and methods

Materials

Mature bananas were purchased from a fruit store (Tehran, Iran). ZnO nanoparticles were bought from NAMAGO Company (Tehran, Iran). Ethylenediaminetetraacetic acid (EDTA, 99.995% purity), p-Benzoquinone (BQ, reagent grade $\geq 98\%$), sodium persulfate ($\text{Na}_2\text{S}_2\text{O}_8$, $\geq 99\%$), potassium iodide (KI, $\geq 99\%$), potassium hydroxide (KOH, $\geq 85\%$), sodium bromate (NaBrO_3 , $\geq 99.5\%$), hydrogen peroxide (H_2O_2 , 32%), sodium azide (NaN_3 , $\geq 99\%$), ethanol ($\geq 99.9\%$), sodium sulfate (Na_2SO_4 , $\geq 99\%$), potassium bicarbonate (KHCO_3 , 99.7%), sodium nitrate (NaNO_3 , $\geq 99\%$), sodium fluoride (NaF, $\geq 99.0\%$), sodium chloride (NaCl, $\geq 99.0\%$), hydrochloric acid (HCl, 37%), calcium sulfate ($\text{CaSO}_4 \cdot 0.2\text{H}_2\text{O}$ ($\geq 99.0\%$), and aluminum sulfate ($\text{Al}_2\text{SO}_4 \cdot 3.18\text{H}_2\text{O}$ (98.0%) were purchased from Merck.

Synthesis of BPAC, BPAC/ZnO nanocomposite

Tap and distilled water were used to wash the dirt and impurities of the banana peels. The banana peels were then chopped into small pieces and were dried in a laboratory oven at 100 °C for 48 h. Next, the banana peels were pulverized and then sieved through a laboratory sieve (200 μ). This powder was then carbonized at a temperature of 550 °C in a nitrogen gas muffle furnace for 1 h. KOH

(45% aqueous solution) was used for activation, with a weight ratio of 1:4 of carbonized material to KOH. After 12 h of agitation on a magnetic stirrer, drying took place for 48 h in a laboratory oven at 120 °C. After drying, the sample was placed in a nitrogen gas muffle furnace at 750 °C for 1 h. Eventually, the BPAC was obtained after washing and neutralizing the pH (Mohammed and Chong 2014).

The physical mixing method was used to synthesize BPAC/ZnO nanocomposites. Different weight ratios (BPAC:ZnO) were used to synthesize this nanocomposite. A certain amount of BPAC was added to 100 ml of distilled water and stirred on a magnetic stirrer for 15 min. Furthermore, a certain amount of ZnO was added to 100 ml of distilled water and stirred for 15 min. Then, the ZnO solutions were added to the BPAC solution under continuous stirring and agitated for 2 h. Following this, the resulting solution was transferred to an ultrasonic bath for 2 h at 70 °C. Finally, the BPAC/ZnO nanocomposite was obtained after washing and drying with ethanol and distilled water (Alhan et al. 2019).

Characterization

The X-ray diffraction (XRD) was analyzed by PW1730, PHILLIPS, Netherlands. The microscopic morphology of the samples was analyzed by FESEM, MIRA III, TESCAN, Czech Republic. The specific surface area of the samples was calculated according to BET, BELSORP MINI II, BEL company, Japan. A Fourier transform infrared spectroscopy (FTIR) was obtained using the AVATAR model of Thermo company, USA.

Evaluation of the AB25 photocatalytic activity

Photocatalytic degradation of AB25 was carried out in a lab-scale reactor (10 cm diameter, 28 cm height, 5 mm thickness, two UVB lamps, and two aerator stones). The evaluation of activity was firstly studied by the optimization of effective parameters in different ranges of parameters. All the experiments were carried out for 150 min. Dark adsorption was conducted for 30 min to establish an adsorption–desorption equilibrium. To determine whether the pollutant concentration declines over time or not, 5 ml of the solution was taken and centrifuged at different time intervals. The concentration of AB25 was analyzed on a UV–Vis spectrophotometer at a wavelength of 602 nm. (Hach, DR4000). Experiments were carried out according to the OFAT method. Tests were performed three times with a maximum error rate of 5%. Also, to calculate the energy consumption of the system, Eq. 1 was used:



$$\frac{\text{Energy consumption} \left(\frac{\text{kWh}}{\text{kg}} \right)}{\text{Concentration}} = \frac{(W_{\text{aeration}} + W_{\text{lamps}} + W_{\text{fan}})t}{V(C_0 - C_t)} \quad (1)$$

Scavenging and inorganic ion investigations were accomplished under optimal conditions for effective parameters. The role of different reactive species and inorganic ions at different concentrations was investigated in the photocatalytic degradation of AB25.

Results and discussion

Characterization

Figure 1 displays the outcomes of the XRD analysis of the BPAC/ZnO nanocomposite. The aromatic zone in the graphitic structure of activated carbon is shown as a small peak in the XRD spectrum between $2\theta = 20\text{--}30^\circ$. This peak is associated with (002) graphitic plane reflections of microcrystals that resemble graphite in activated carbon. This peak also shows that high porosity activated carbon has amorphous characteristics (Patel et al. 2021). The low BPAC peak was caused by the dominance of zinc oxide in the sample. Sharp diffraction peaks and no additional diffraction peaks were present, showing that the sample demonstrated high purity and crystallinity (Xu et al. 2022). Major ZnO peaks were detected at $2\theta = 31.95^\circ, 34.55^\circ, 36.45^\circ, 47.8^\circ, 56.8^\circ, 63.15^\circ, 66.75^\circ, 68.15^\circ, 69.3^\circ, 72.75^\circ, 77.1^\circ$; which can be denoted as (100), (002), (101), (102), (110), (103), (200), (112), (201), (004), and (202) respectively.

FTIR analysis was utilized to identify and describe the chemical compounds and groups inside the samples' structures. Figure 2 indicates an absorption peak relating

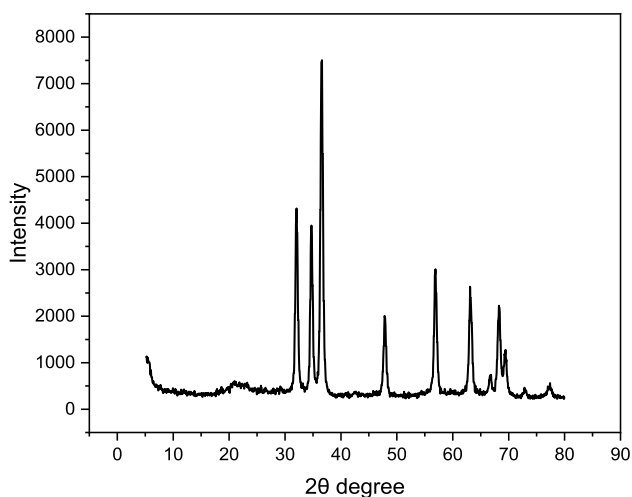


Fig. 1 XRD pattern of BPAC/ZnO

to tensile vibrations of --OH at 3434.20 cm^{-1} . Also, the 2924.05 cm^{-1} peak corresponds to C--H stretching. The wavenumbers of 1638.10 cm^{-1} and 1384.14 cm^{-1} were assigned to the C=C and C--H bonds. The wavenumber at 1071.70 cm^{-1} was ascribed to the C--O alcohol groups (Foroutan et al. 2022). Zn--O moiety's stretching band was observed at 469.40 cm^{-1} in the BPAC/ZnO sample (Fatima et al. 2022).

The morphology of the prepared samples was characterized by Field Emission Scanning Electron Microscopy (FESEM), the results of which are presented in Fig. 3. Activated carbon contained a pore-like structure, which could provide a good place for the incorporation of the ZnO particles (Fig. 3a, b). Also, ZnO nanoparticles showed quite uniform particle size and shape, and the hexagonal structure of zinc oxide particles is quite clear (Fig. 3c, d). In Fig. 3e, f the successful formation of activated carbon and zinc oxide can be seen. The BPAC surface morphology was altered following the uniform loading of zinc oxide particles (Amir et al. 2022).

Nitrogen adsorption/desorption isotherms of BPAC and BPAC/ZnO were measured to examine the BET surface area and pore size distribution (Table 1). The specific surface area and total pore volume of the BPAC ($712.28\text{ m}^2\text{ g}^{-1}$ and $0.3351\text{ cm}^3\text{ g}^{-1}$, respectively) were higher than those of BPAC/ZnO nanocomposite ($321.1\text{ m}^2\text{ g}^{-1}$ and $0.1168\text{ cm}^3\text{ g}^{-1}$, respectively). A high surface area of BPAC provides active sites that facilitate the diffusion of polluting products and reaction inside or outside the BPAC/ZnO photocatalyst, leading to an increase in the photocatalytic activity (Leichtweis et al. 2020). Moreover, the mean pore diameters of BPAC and BPAC/ZnO were obtained 2.089 nm and 3.946 nm, respectively. The loading of ZnO nanoparticles on the BPAC surface lowered the total pore volume of the BPAC/ZnO nanocomposite while increasing the mean pore diameter. This is because the BPAC pores were occupied by the ZnO nanoparticles (Table 2).

Optimization of effective parameters

To achieve the best possible results, the mixing ratio of the synthesized nanocomposite (BPAC:ZnO) was changed, and the removal efficiency was evaluated. A 150 min experiment was conducted. Dark adsorption was conducted for 30 min to establish an adsorption–desorption equilibrium. According to the results, when a higher proportion of BPAC was included in the nanocomposite, the adsorption capacity was improved. The results can be correlated to the surface area of the nanocomposite. In order to determine the optimal mixing ratio, a study of energy consumption was also conducted. Results showed that the 3:7 mixing ratio demonstrated the highest removal efficiency and the lowest energy consumption; therefore, it was selected as the optimum mixing ratio.

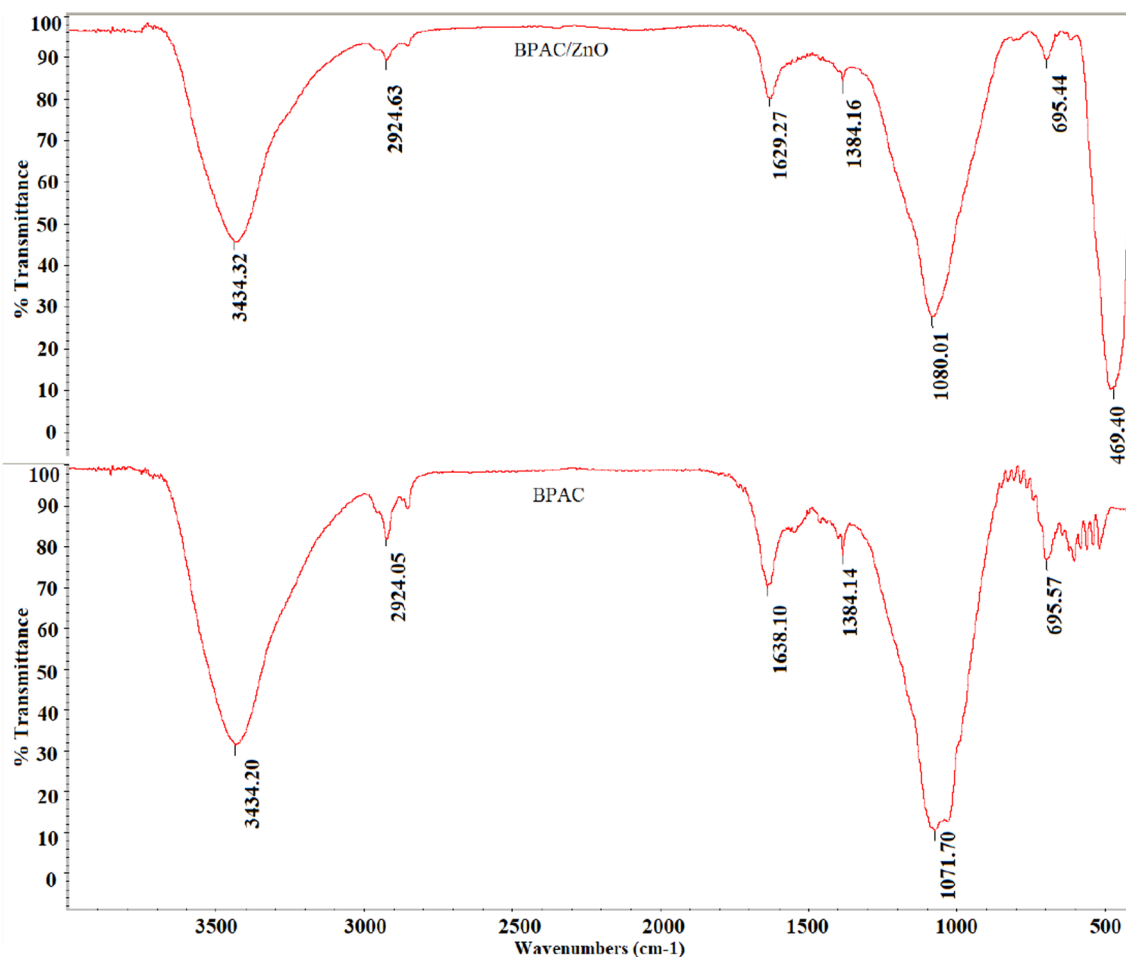


Fig. 2 Fourier transform infrared (FTIR) spectrum of the of BPAC and BPAC/ZnO

The initial pH value strongly influences the photocatalytic degradation efficiency and surface charge of the nanocomposite. Based on the results, higher removal efficiency occurs at lower pHs on account of the anionic structure of AB25 dye and the positive surface charge of the nanocomposite at a pH lower than pH_{pzc} of the nanocomposite, which was 6.8. The dye molecules adhered to the nanocomposite surface due to the electrostatic attractions of the nanocomposite surface and the AB25 molecules. Furthermore, hydroxyl radicals are more capable of oxidizing organic pollutants at low pH values compared to basic pH levels (Munagapati et al. 2018). Eventually, energy consumption calculations were carried out, and $pH = 5$ was determined as the optimal pH.

Generally, the dye removal efficiency decreases as the dye concentration rises. The nanocomposite active sites, consequently, were saturated with contaminants, reducing the efficiency of photocatalytic degradation. In the presence of high concentrations of AB25, fewer dye molecules made contact with the photocatalyst surface, resulting in lower photodegradation (Suresh and Sivasamy 2020). Furthermore, when dye concentration is high, the light is absorbed by the dye

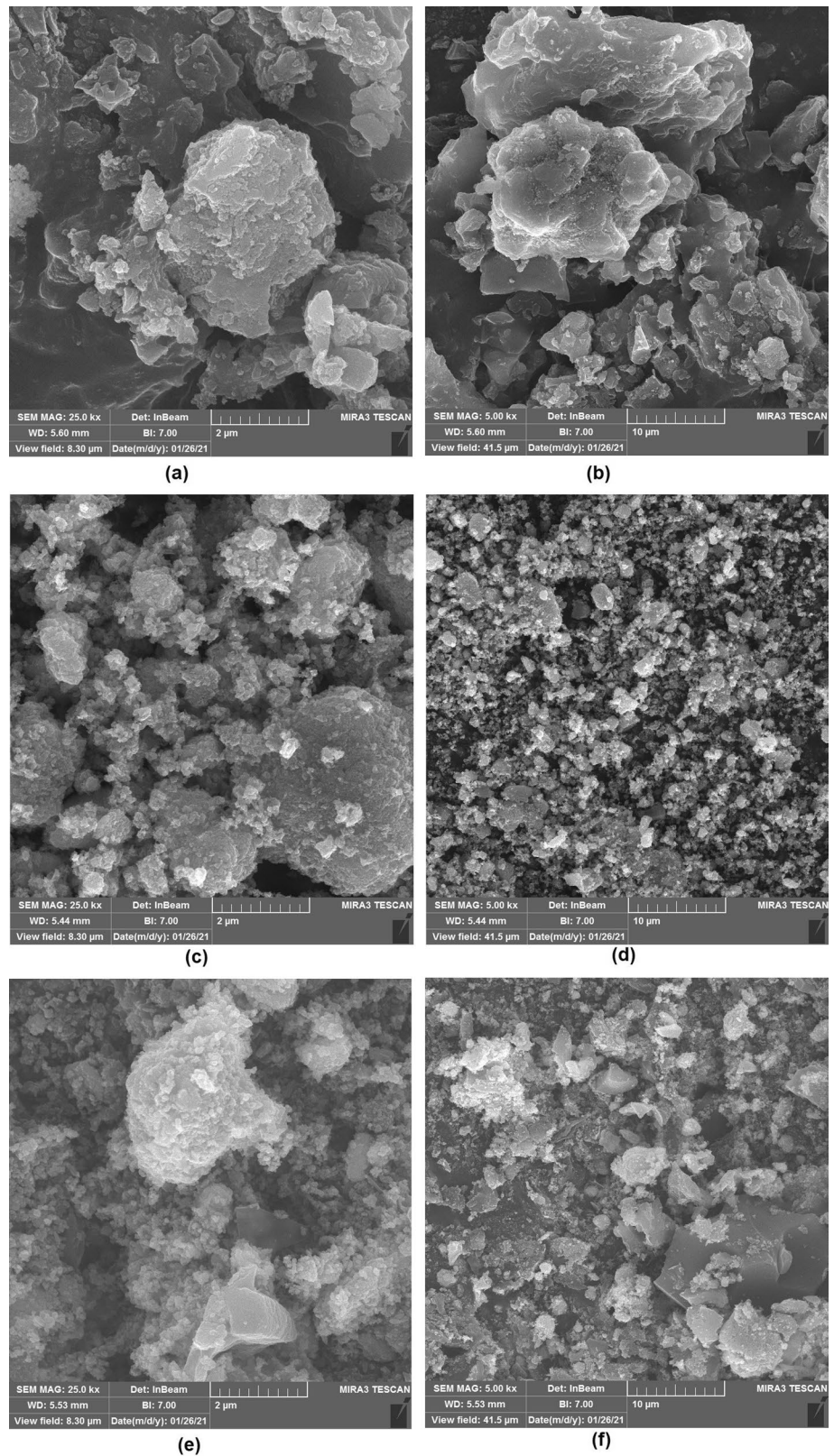
molecules before it reaches the nanocomposite surface. As a result, the generation of hydroxyl radicals is reduced. Finally, based on the calculations for energy consumption, 150 mg L^{-1} was selected as the optimum dye concentration.

The removal of dye is increased by increasing nanocomposite concentration. Based on the results of the study, the removal efficiency improved from 77 to 93% by increasing the nanocomposite from 0.2 g L^{-1} to 0.7 g L^{-1} . This can be associated with the small amount of nanocomposite, which is inadequate to generate enough reactive species such as superoxide and hydroxyl radicals to reach a sufficient removal efficiency. The number of photocatalytic particles in the reactor increases when a high amount of the nanocomposite is added to the system (Suresh and Sivasamy 2020). Consequently, the active adsorption sites on the surface are multiplied, enhancing superoxide and hydroxyl radical generation and facilitating better photocatalytic degradation. Therefore, 0.6 g L^{-1} of nanocomposite was selected as the optimal dosage.

Dissolved oxygen plays a crucial role in the degradation of organic materials. The electron–hole recombination



Fig. 3 FESEM images of BPAC (a,b), ZnO (c,d), and BPAC/ZnO (e,f)



in photocatalytic processes is essential for energy waste. Oxygen molecules can function as electron acceptors and separate electrons from holes, reducing the likelihood of

electron–hole recombination. Therefore, electron acceptors facilitate the separation of photogenerated electrons and holes in the photocatalytic process, leading to better



Table 1 Physical properties of Banana peel activated carbon and BPAC/ZnO nanocomposite

Sample	S _{BET} (m ² /g)	V _{Total} (cm ³ /g)	D _p (nm)
Banana peel activated carbon	712.28	0.3351	2.089
BPAC/ZnO	321.1	0.1168	3.946

photocatalytic performance (Thor et al. 2020). In fact, superoxide radicals are generated in the system and provide enough oxygen for photo-electron evacuation. Finally, the 5 L min⁻¹ aeration rate showed the lowest energy consumption, and it was selected as the optimal value.

Photocatalytic degradation of contaminants is greatly influenced by UV light intensity. According to the results, the removal rates of AB25 were directly related to the intensity of UV light. As the light intensity increased, the number of photons increased, resulting in great light absorption by the photocatalyst surface (Mirmasoomi et al. 2017).

Eventually, the 16W UV intensity was determined as the optimum value.

Scavenger experiments

The influence of different concentrations of several scavengers on the photocatalytic degradation of AB25 under the optimal condition of the effective parameters was accomplished. Potassium iodide (KI) and sodium azide (NaN₃) as hydroxyl radical scavengers ([•]OH), ethanol and EDTA as photogenerated holes (h⁺), H₂O₂, Na₂S₂O₈, and NaBrO₃ as electron scavengers (e⁻), and p-BQ as a superoxide radical scavenger (O₂^{•-}) were used in this work. The concentrations of the scavengers used in this study were 3, 10, and 30 mM. The results of scavenger tests are presented in the figures below.

It is evident that with 1, 3, and 10 mM of EDTA, the photocatalytic removal efficiency dwindled to 80%, 65%, and 59%, respectively. Also, it decreased to 84%, 73%, and 68% when ethanol was added to the solution. The results are

Table 2 Results of the optimization of the effective parameters on photocatalytic degradation of AB25

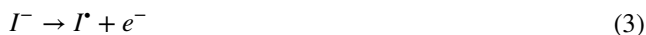
Parameter	Values	Other parameters	Dye removal (%)	Energy consumption (KWh kg ⁻¹)	Optimum value
BPAC:ZnO nanocomposite mixing ratio	1:9	(Aeration rate) = 5 L/min, (Dye) = 100 mg/L, (pH) = 6.9 neutral, (UV light intensity) = 16W, (Nanocomposite concentration) = 0.2 g/L	49	1593	3:7
	2:8		49.7	1602	
	3:7		54	1503	
	4:6		53	1514	
	5:5		53	1517	
pH	3	(Mixing ratio) = 3:7, (Nanocomposite concentration) = 0.4 g/L, (Dye) = 100 mg/L, (Aeration rate) = 5 L/min, (UV light intensity) = 16W	92	968	5
	5		93	962	
	6.9		87	1012	
	9		81	1072	
	11		78	1112	
Dye concentration (mg/L)	100	(UV light intensity) = 16W, (Mixing ratio) = 3:7 (Nanocomposite concentration) = 0.4 g/L, (pH) = 5, (Aeration rate) = 5 L/min	93	959	150
	150		88	665	
	200		75	672	
	250		62	712	
Nanocomposite concentration (g/L)	0.2	(Dye concentration) = 150 mg/L, (Aeration rate) = 5 L/min, (Mixing ratio) = 3:7, (UV light intensity) = 16W, (pH) = 5	77	747	0.6
	0.4		88	665	
	0.5		92	645	
	0.6		94	631	
	0.7		93	638	
	0.9		97	620	
Aeration rate (L/min)	2.5	(Nanocomposite concentration) = 0.6 g/L, (Mixing ratio) = 3:7, (pH) = 5, (UV light intensity) = 16W, (Dye concentration) = 150 mg/L	90	656	5
	5		94	631	
	7		91	645	
UV intensity (W)	8	(Nanocomposite concentration) = 0.6 g/L, (Mixing ratio) = 3:7, (pH) = 5, (Aeration rate) = 5 L/min, (Dye concentration) = 150 mg/L	80	721	16
	16		93	630	



presented in Fig. 4. In the presence of EDTA and ethanol, the removal efficiency declined, indicating that the valence band holes which produce hydroxyl radicals have an important role in the degradation of AB25. The presence of EDTA and ethanol in the system, as a result, decreased the holes and the $\cdot\text{OH}$ radicals, which eventually translated into a diminution in removal efficiency.

Then, the dye removal efficiency was decreased by adding 3, 10, and 30 mM NaN_3 and KI as hydroxyl radical scavengers. It was decreased to 92%, 90%, and 85% when different concentrations of NaN_3 were introduced to the solution. The addition of KI, furthermore, led to depletion in removal efficiency, which was 91%, 89%, and 82% for 3, 10, and 30 mM, respectively. The results are presented in Fig. 5. KI contains an (I^-) ion that reacts with hydroxyl radicals and holes (Eq. 2–6), which causes a decrease in the removal efficiency (Li et al. 2011). In light of this, $\cdot\text{OH}$ radicals played a supplementary role in the photocatalytic degradation process. Also, the decrease in AB25 removal efficiency due to the

presence of NaN_3 could be linked to the reaction of NaN_3 with singlet oxygen and hydroxyl radical.



According to the results, after adding 2 mM of $\text{Na}_2\text{S}_2\text{O}_8$, H_2O_2 , and NaBrO_3 to the photocatalytic reactor, the removal efficiency improved to 95%, 96%, and 96%, respectively. While by adding 10 mM of $\text{Na}_2\text{S}_2\text{O}_8$ and NaBrO_3 , the removal

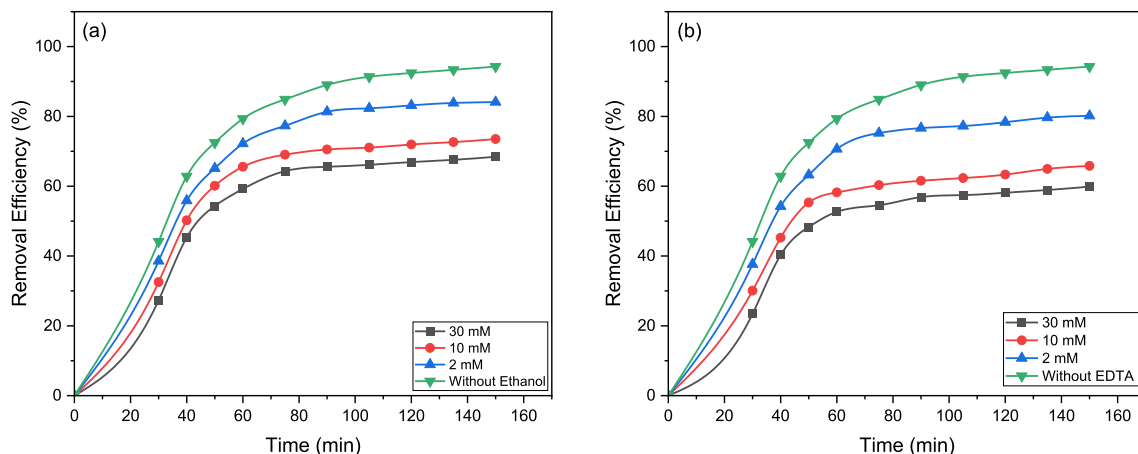


Fig. 4 Changes in AB25 removal efficiency in the existence of ethanol (a) and EDTA (b)

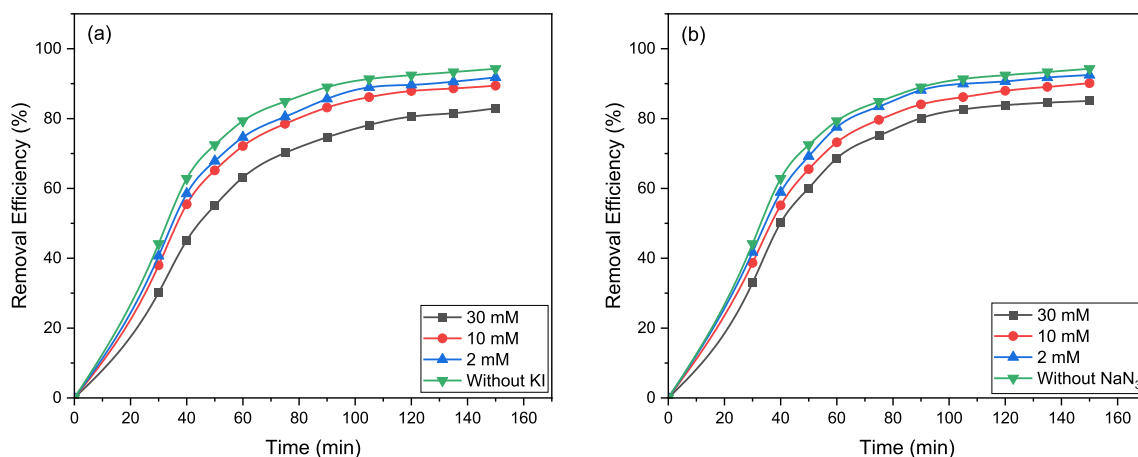
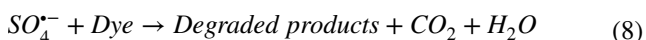
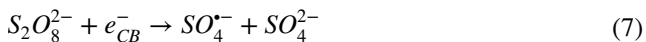
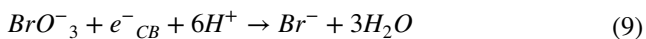


Fig. 5 Effect of different concentrations of KI (a) and NaN_3 (b) on the photocatalytic degradation of AB25

efficiency increased to 96% and 99%, the removal efficiency dwindled to 86% when 10 mM of H₂O₂ was added. Likewise, by adding 30 mM of Na₂S₂O₈ and NaBrO₃, the removal efficiency improved to 98% and 99%, whereas the removal efficiency reduced to 78% in the presence of 30 mM of H₂O₂. The results are presented in Fig. 6. Due to Na₂S₂O₈ ability to create sulfate radicals (SO₄^{•-}), using Na₂S₂O₈ increased the efficiency of the process (Eq. 7 and 8.) (Govindan et al. 2017).



Also, the electron and the bromate ion reaction reduced the electron–hole recombination, improving the removal efficiency (Eq. 9.) (Makama et al. 2020).



This increase in removal efficiency indicates the positive effect of bromate ions on dye removal by trapping electrons. The presence of H₂O₂ in the process could increase the efficiency, but in this study, it reduced the removal efficiency of AB25 due to its possible reaction with the hydroxyl radicals (Eq. 10 and 11) (Govindan et al. 2017).



In this reaction, a hydroperoxyl radical was produced, which consumed the hydroxyl radical (Monteagudo et al. 2020). Therefore, it can reduce removal efficiency. If the concentration of H₂O₂ exceeds a certain level, it could lead to a diminution in removal efficiency. In this study, the concentration of 10 and 30 mM H₂O₂ caused a reduction in efficiency from 94 to 86% and 78%. The results are presented in Fig. 6a.

Eventually, the effect of p-BQ was investigated. In the presence of photogenerated electrons, oxygen molecules

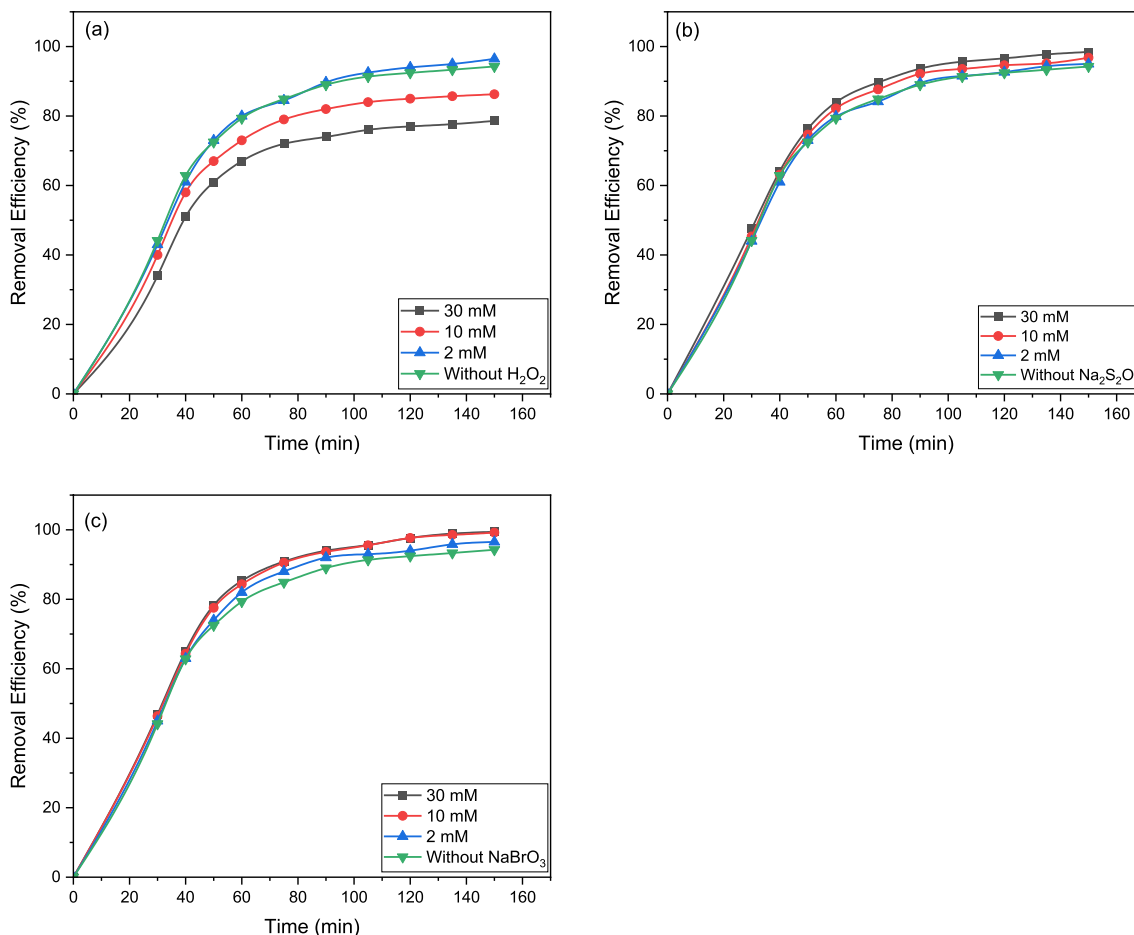


Fig. 6 Changes in removal efficiency of AB25 in the presence of H₂O₂ (a), Na₂S₂O₈ (b), and NaBrO₃ (c)

are reduced to a superoxide anion (O_2^-). p-BQ was capable of capturing O_2 radicals (Silvestri et al. 2019). It can consequently decrease degradation rates, showing the existence of O_2 radicals in the reactor (Eq. 12.) (Palominos et al. 2008). Based on the results, dye removal efficiency reduced from 94 to 68% and 49% in the presence of 2 and 10 mM of p-BQ in the solution. The results are presented in Fig. 7.



According to the above results, it is worth mentioning that superoxide radicals and photo-generated holes have a decisive role in the photocatalytic degradation of AB25. When p-BQ was used as superoxide radical scavengers, the photocatalytic degradation of AB25 was significantly inhibited by O_2 radicals. Moreover, photo-generated holes can produce $\cdot OH$ radicals, and the production of $\cdot OH$ radicals was reduced in the presence of EDTA and ethanol, which led to a diminution in AB25's removal efficiency. In addition, electron acceptors, two examples of which are $Na_2S_2O_8$ and $NaBrO_3$, accelerated the degradation of AB25. As a result, SO_4^- and BrO_3^- oxidants are capable of decomposing AB25. Also, the presence of H_2O_2 in the solution caused a reduction in the photocatalytic performance. Furthermore, the results of the study revealed that KI and NaN_3 had a low impact on AB25 degradation. Therefore, it is worth noting that in the photocatalytic degradation of AB25, hydroxyl radicals played a supplementary role.

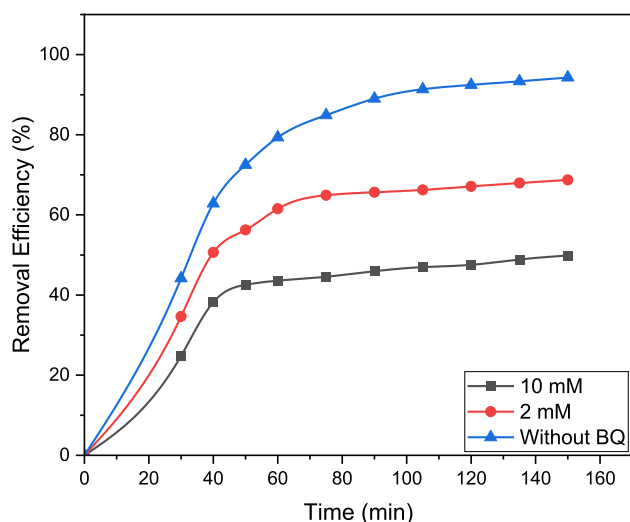


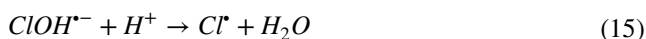
Fig. 7 Impact of various concentrations of BQ on the removal efficiency of AB25

Effect of inorganic ions

Effect of anions

Salts are usually found in aqueous media, and a number of researchers claim that the inorganic salts in water play an important role in the photocatalytic degradation process of organic compounds. In order to investigate the anion effect, the impact of several anions (Cl^- , HCO_3^- , NO_3^- , and F^-) on the photocatalytic degradation of AB25 was investigated.

Cl^- inhibited the photocatalytic degradation of AB25, and the inhibitory effect improved by increasing Cl^- concentration. Regarding the pH_{pzc} of BPAC/ZnO, the catalyst's surface was positively charged when the pH of the solution was lower than 6.8. Consequently, anions such as Cl^- could be adsorbed on the surface of the nanocomposite and block the active sites, which results in the reduction of the removal efficiency. Moreover, I^- in the chloride is an excellent scavenger for valence band holes. Therefore, Cl^- could also react with the valence band hole and compete with AB25 for the holes, decreasing the photocatalytic degradation rate. The effect of chloride ions is given by (Eq. 13–16) (Santiago et al. 2014). During the degradation of organic compounds, chloride anions act as effective inhibitors. In this study, the removal efficiency dwindled from 94 to 93%, 90%, and 85% by adding 2, 10, and 30 mM NaCl to the solution, respectively (Fig. 8a). In order to confirm the adsorption of Cl^- onto the nanocomposite surface, once the process completed, FT-IR analysis was conducted, and the results are presented in Fig. 10b.



Fluoride also would inhibit the production of $\cdot OH$ radicals by covering the nanocomposite surface. As a result, when F^- was present in the solution, the degradation was predominantly caused by $\cdot OH$ radicals. Participation of holes and surface hydroxyl radicals in photocatalytic degradation could occur in the absence of F^- (Dugandžić et al. 2017). As can be seen in Fig. 8b, based on the differences between the reaction rates in the absence and presence of F^- anions, it should be noted that holes and surface hydroxyl radicals are involved in the photocatalytic degradation of AB25. In this study, the removal efficiency decreased from 94 to 93%, 84%, and 80% by adding 2, 10, and 30 mM NaF to the AB25 solution, respectively (Fig. 8b).

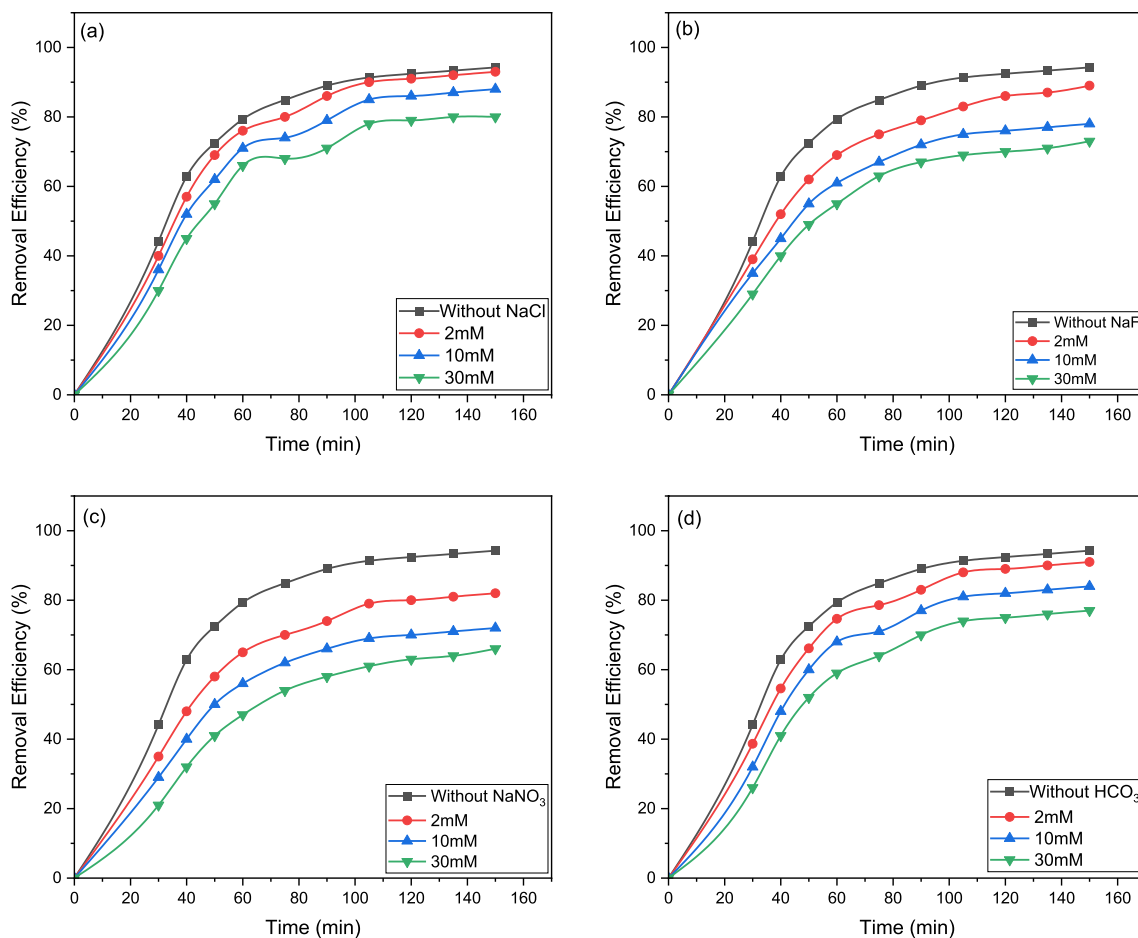
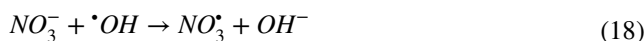


Fig. 8 Changes in removal efficiency of AB25 in the existence of different concentrations of inorganic anions

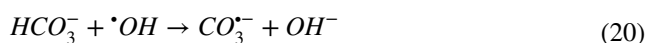
The inhibition effect of NO_3^- was much greater than that of Cl^- . In the presence of low concentrations of nitrate anions (below 0.1 mM), the degradation of pollutants can be improved (Dugandžić et al. 2017). NO_3^- ions could be adsorbed on the nanocomposite surface and compete for the active sites when excessive amounts of this ion were available in the solution. It was observed that the removal efficiency was inhibited at higher concentrations of NO_3^- in this study. The inhibition was much more significant than chloride anions on account of the larger size of NO_3^- anions, which led to a more effective blocking of the nanocomposite surface. The photocatalytic degradation efficiency was reduced from 94 to 89%, 82%, and 75% by adding 2, 10, and 30 mM NaNO_3^- to the solution, respectively (Fig. 8c). Also, nitrate anion could act as radical scavengers by reacting with holes and hydroxyl radicals (Eq. 17 and 18) (Dugandžić et al. 2017). Also, to confirm the adsorption of NO_3^- onto the BPAC/ZnO surface, FT-IR analysis was carried out after the completion of the process, the result of which is presented in Fig. 10d. Reduction at bands 3400 cm^{-1} and 1600 cm^{-1}

showed that NO_3^- was adsorbed onto the surface of BPAC/ZnO nanocomposite.

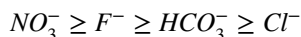


When HCO_3^- reacted with $\cdot\text{OH}$, carbonate radicals, which are weak oxidizing reagents and rarely react with other organic molecules, were formed (Santiago et al. 2014). The photocatalytic degradation of AB25 was mainly due to $\text{O}_2^{\cdot-}$, not due to OH . Thus, HCO_3^- had an inconsiderable inhibitory effect on degradation. The removal efficiency decreased from 94 to 92%, 88%, and 82% by adding 2, 10, and 30 mM KHCO_3^- to the solution, respectively (Fig. 8d). It has been reported that bicarbonate ions can scavenge h^+ and other radicals based on the reactions given below (Santiago et al. 2014).





Finally, inorganic additives inhibit the photocatalytic removal of AB25 in the following order:



Effect of cations

Wastewaters contain numerous cations of different metals. These ions, including K^+ , Na^+ , Ca^{2+} , and Mg^{2+} , can affect photocatalytic degradation (Dugandžić et al. 2017). In this

study, the photocatalytic degradation of AB25 was studied in the presence of different concentrations of Ca^{2+} and Al^{3+} cations. These two salts exhibited an inhibition effect on the AB25 photocatalytic degradation. In this study, the removal efficiency was reduced from 94 to 87%, 82%, and 68% by adding 2, 10, and 30 mM $(\text{Al}_2\text{SO}_4)_3$ to the AB25 solution, respectively (Fig. 9). Also, the removal efficiency dwindled from 94 to 90%, 85%, and 83% by adding 2, 10, and 30 mM (CaSO_4) to the AB25 solution, respectively. AB25 was strongly inhibited by aluminum ions in photocatalytic degradation, resulting from Al^{3+} adsorption. Calcium ions had a similar impact on the photocatalytic degradation rate to Al^{3+} . Although the nanocomposite surface and Al^{3+} were

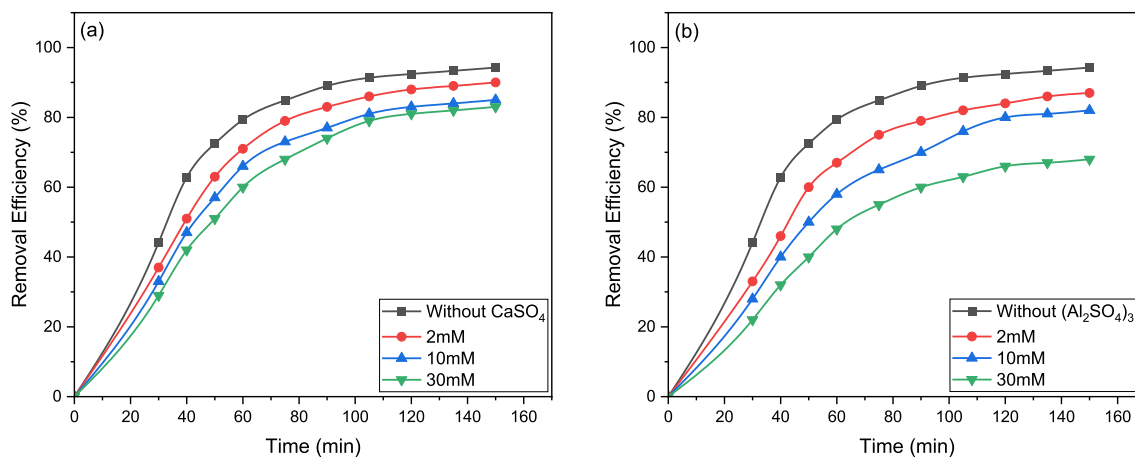


Fig. 9 Effect of different concentrations of (CaSO_4) and $(\text{Al}_2\text{SO}_4)_3$ on the photocatalytic degradation of AB25

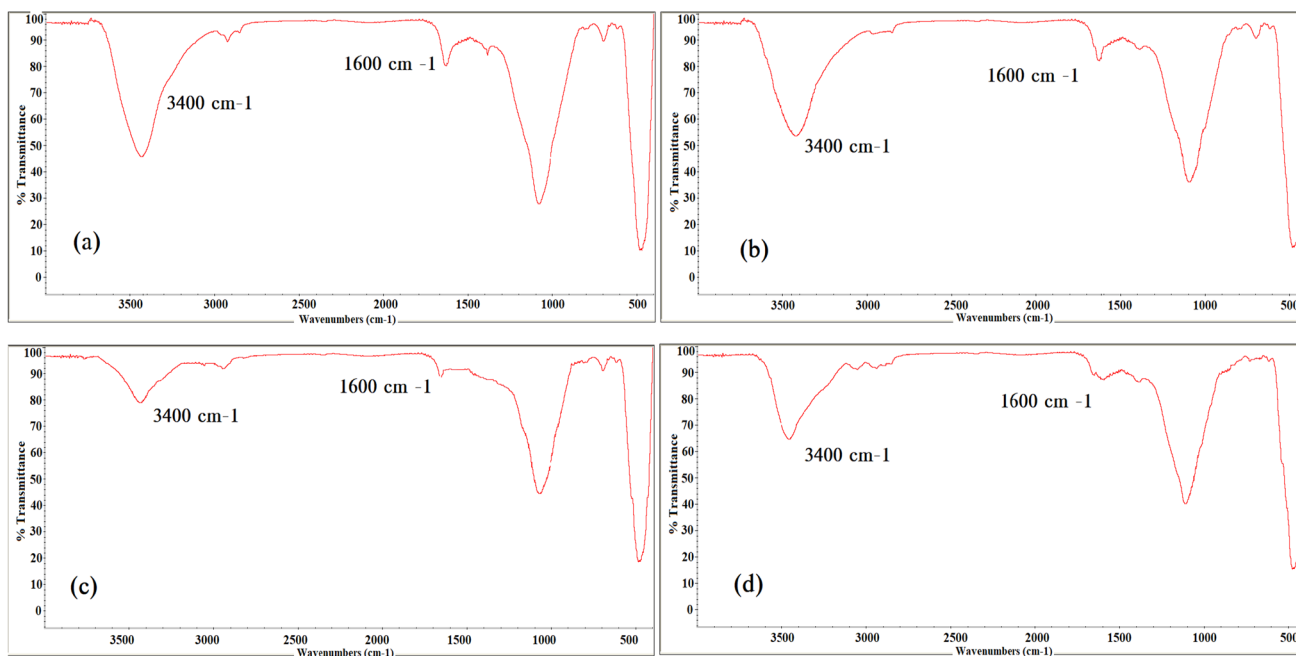


Fig. 10 FT-IR spectrum of BPAC/ZnO nanocomposite (a), changes in FT-IR spectrum after adsorption of Cl^- (b), Al^{3+} (c), and NO_3^- (d)



charged positively when the pH value was below the pH_{pzc} of the nanocomposite, Al^{3+} adsorption occurred. Also, after the completion of the process, FT-IR analysis was carried out to confirm the adsorption of Al^{3+} onto the BPAC/ZnO surface. The results are presented in Fig. 10b. The FTIR spectra ensured a reduction at bands 3400 cm^{-1} and 1600 cm^{-1} when Al^{3+} was adsorbed on the nanocomposite.

Photocatalytic mechanism

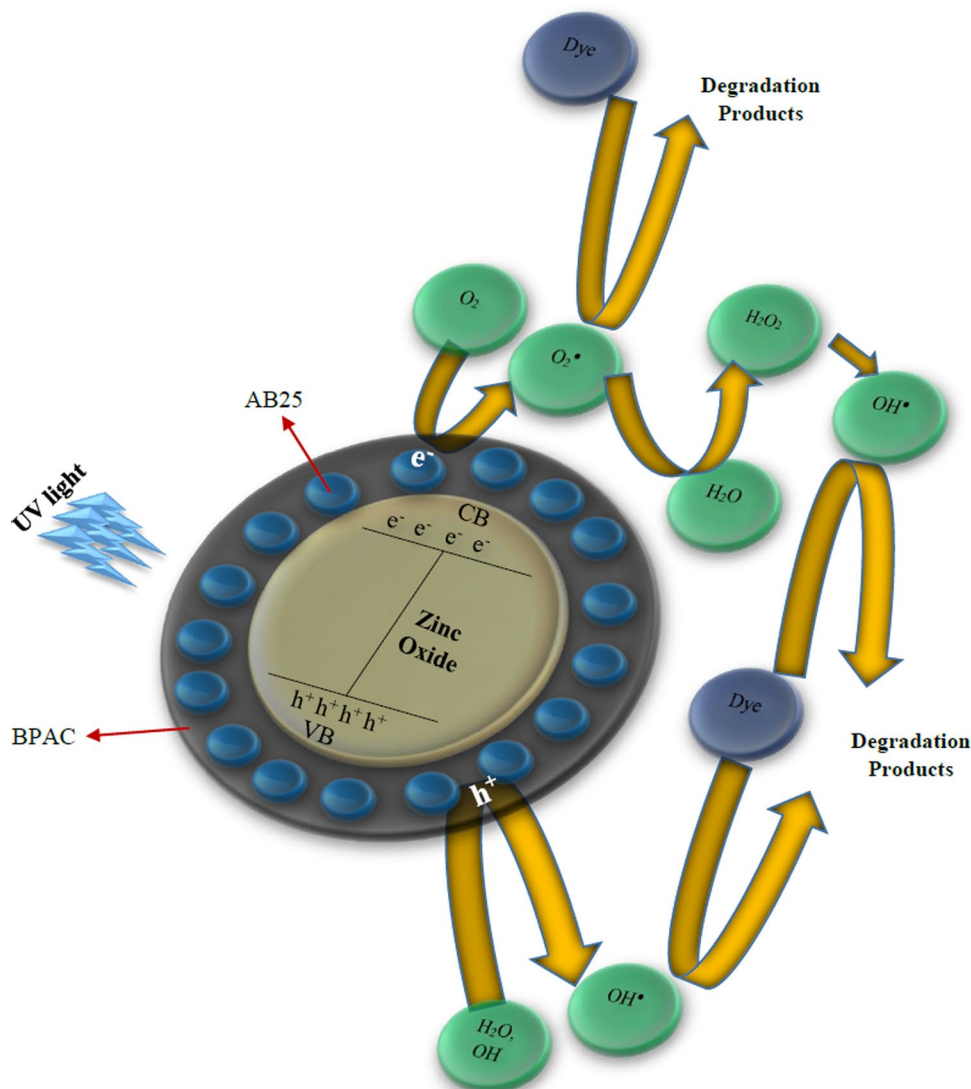
The mechanism of AB25 photocatalytic degradation by BPAC/ZnO nanocomposite is illustrated in Fig. 11. BPAC's pore structure caused the adsorption of AB25 molecules. Because of this, there was a greater opportunity for photocatalysts to interact with pollutants. The generated e^- and h^+ experienced a transition to the photocatalyst surface during the photocatalytic process. When an electron traveled to the photocatalyst surface, O_2 was converted to $O_2^{\cdot-}$. The

hole also oxidized H_2O into OH^{\cdot} when moved to the catalyst surface. It is important to note that electron–hole recombination on the photocatalyst surface reduced the removal efficiency. The photocatalytic process reached a higher efficiency when electron–hole recombination was prevented. Considering that BPAC acts as an electron acceptor in the photocatalytic system, it inhibits electron–hole recombination. The electrons could have a reaction with O_2 , leading to the production of many oxidizing radicals like $O_2^{\cdot-}$ and OH^{\cdot} (Lu et al. 2019). Eventually, final products such as CO_2 and H_2O were produced because of the disintegration of AB25 molecules into smaller products.

UV–visible spectra changes

Figure 12 shows the absorption spectral changes when the synthesized nanocomposite degrades the AB25 aqueous solution. As shown in Fig. 12, wavelengths at 305 nm,

Fig. 11 Photocatalytic mechanism of AB 25 by BPAC/ZnO nanocomposite



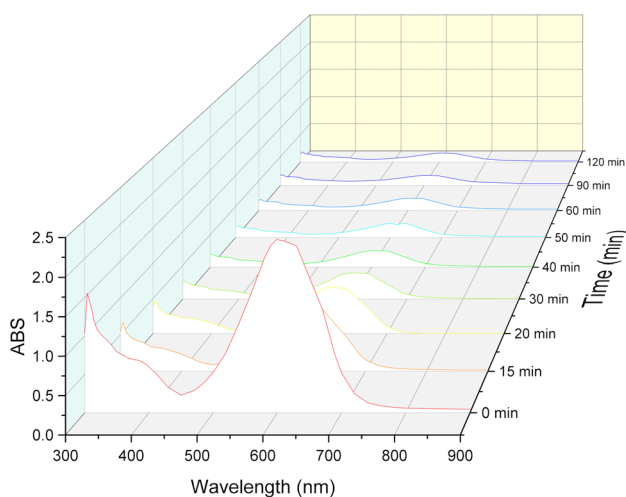


Fig. 12 Absorption spectral changes of AB25 aqueous solution during the photocatalytic process

394 nm, and 602 nm were allotted to AB25 maximum wavelengths. Peaks at 390 nm and 305 nm were attributed to carbonyl and benzene, respectively. The main peak at 602 nm was associated with the anthraquinone chromophoric group. Figure 12 indicates the diminution of AB25 wavelengths, informing that the benzene rings were broken up on account of photocatalytic degradation. The AB25 anthraquinone structure, moreover, was broken down because of the O_2^- , h^+ , and OH^- produced in the system.

Conclusion

The photocatalytic decomposition of Acid Blue 25 by BPAC/ZnO nanocomposite was investigated. The findings indicated an elimination efficacy of 94% after 150 min under optimally effective conditions. Under the optimal conditions of effective parameters, the impact of several reactive species on photocatalytic degradation of AB25 was examined. The results showed that h^+ and O_2^- played a major role, while hydroxyl radicals played an auxiliary role in the photocatalytic degradation of AB25. The presence of electron scavengers such as $Na_2S_2O_8$ and $NaBrO_3$ increased the degradation rate. Also, the impact of inorganic anions and cations on the photocatalytic degradation of AB25 was examined. Among the anions, NO_3^- exhibited the greatest inhibition ability. Inorganic anions inhibited the removal efficiency of AB25 in the following order $NO_3^- \geq F^- \geq HCO_3^- \geq Cl^-$. Similarly, Al^{3+} showed the highest inhibition capacity among other cations.

Acknowledgements The authors wish to thank all who assisted in conducting this work.

Availability of data and materials Not applicable.

Declarations

Conflict of interest The author declares that he has no known competing financial interests or personal relationships that could have appeared to influence the work reported in this paper.

Ethical approval The manuscript has not been previously published, is not currently submitted for review to any other journal, its publication is approved by all authors and tacitly or explicitly by the responsible authorities where the work was carried out. It will not be submitted elsewhere before this journal makes a decision, and if accepted, it will not be published elsewhere in the same form or any other language, including electronically, without the written consent of the copyright holder.

Consent to participate Authors have mutual consent in this submitted work.

References

- Ahmadian A, Goharrizi BA, Shahriari T, Ahmadi S (2022) Adsorption of chromium (VI) and acid orange 7 on lemon peel biochar: a response surface methodology approach. *Int J Environ Sci Technol*. <https://doi.org/10.1007/s13762-022-04726-3>
- Alhan S, Nehra M, Dilbaghi N et al (2019) Potential use of ZnO@activated carbon nanocomposites for the adsorptive removal of Cd²⁺ ions in aqueous solutions. *Environ Res* 173:411–418. <https://doi.org/10.1016/J.ENVRES.2019.03.061>
- Amir M, Fazal T, Iqbal J et al (2022) Integrated adsorptive and photocatalytic degradation of pharmaceutical micropollutant, ciprofloxacin employing biochar-ZnO composite photocatalysts. *J Ind Eng Chem*. <https://doi.org/10.1016/J.JIEC.2022.07.050>
- Azzam EMS, Fathy NA, El-Khouly SM, Sami RM (2019) Enhancement of the photocatalytic degradation of methylene blue dye using fabricated CNTs/TiO₂/AgNPs/surfactant nanocomposites. *J Water Process Eng* 28:311–321. <https://doi.org/10.1016/J.JWPE.2019.02.016>
- Babaei AA, Golshan M, Kakavandi B (2021) A heterogeneous photocatalytic sulfate radical-based oxidation process for efficient degradation of 4-chlorophenol using TiO₂ anchored on Fe oxides@carbon. *Process Saf Environ Prot* 149:35–47. <https://doi.org/10.1016/J.PSEP.2020.10.028>
- Brindha R, Rajeswari S, Jennet Debora J, Rajaguru P (2022) Evaluation of global research trends in photocatalytic degradation of dye effluents using scientometrics analysis. *J Environ Manag* 318:115600. <https://doi.org/10.1016/J.JENVMAN.2022.115600>
- Chen SQ, Li M, Ma XY et al (2021a) Influence of inorganic ions on degradation capability of Fe-based metallic glass towards dyeing wastewater remediation. *Chemosphere* 264:128392. <https://doi.org/10.1016/J.CHEMOSPHERE.2020.128392>
- Chen X, Zhou J, Chen Y et al (2021b) Degradation of tetracycline hydrochloride by coupling of photocatalysis and peroxymonosulfate oxidation processes using CuO-BiVO₄ heterogeneous catalyst. *Process Saf Environ Prot* 145:364–377. <https://doi.org/10.1016/J.PSEP.2020.08.016>
- Chhabra VA, Kaur R, Walia MS et al (2020) PANI/PbS QD nanocomposite structure for visible light driven photocatalytic degradation

- of rhodamine 6G. *Environ Res* 186:109615. <https://doi.org/10.1016/J.ENVRES.2020.109615>
- Daimon T, Hirakawa T, Kitazawa M et al (2008) Formation of singlet molecular oxygen associated with the formation of superoxide radicals in aqueous suspensions of TiO₂ photocatalysts. *Appl Catal A Gen* 340:169–175. <https://doi.org/10.1016/J.APCATA.2008.02.012>
- Daneshvar E, Sohrabi MS, Kousha M et al (2014) Shrimp shell as an efficient bioadsorbent for acid blue 25 dye removal from aqueous solution. *J Taiwan Inst Chem Eng* 45:2926–2934. <https://doi.org/10.1016/J.JTICE.2014.09.019>
- Dugandžić AM, Tomašević AV, Radišić MM et al (2017) Effect of inorganic ions, photosensitisers and scavengers on the photocatalytic degradation of nicosulfuron. *J Photochem Photobiol A Chem* 336:146–155. <https://doi.org/10.1016/j.jphotochem.2016.12.031>
- Fatima H, Azhar MR, Zhong Y et al (2022) Rational design of ZnO-zeolite imidazole hybrid nanoparticles with reduced charge recombination for enhanced photocatalysis. *J Colloid Interface Sci* 614:538–546. <https://doi.org/10.1016/J.JCIS.2022.01.086>
- Foroutan R, Peighambaroust SJ, Mohammadi R et al (2022) Cadmium ion removal from aqueous media using banana peel biochar/Fe₃O₄/ZIF-67. *Environ Res* 211:113020. <https://doi.org/10.1016/J.ENVRES.2022.113020>
- Govindan K, Chandran HT, Raja M et al (2017) Electron scavenger-assisted photocatalytic degradation of amido black 10B dye with Mn₃O₄ nanotubes: a response surface methodology study with central composite design. *J Photochem Photobiol A Chem* 341:146–156. <https://doi.org/10.1016/J.JPHOTOCHEM.2017.03.025>
- Guan S-H, Zhao K-F, Tong Q et al (2021) A review of photocatalytic materials application on nonylphenol degradation. *Environ Chall* 4:100172. <https://doi.org/10.1016/J.ENVC.2021.100172>
- Guillard C, Lachheb H, Houas A et al (2003) Influence of chemical structure of dyes, of pH and of inorganic salts on their photocatalytic degradation by TiO₂: comparison of the efficiency of powder and supported TiO₂. *J Photochem Photobiol A Chem* 158:27–36. [https://doi.org/10.1016/S1010-6030\(03\)00016-9](https://doi.org/10.1016/S1010-6030(03)00016-9)
- Huang Y, Sheng B, Wang Z et al (2018) Deciphering the degradation/chlorination mechanisms of maleic acid in the Fe(II)/peroxymonosulfate process: an often overlooked effect of chloride. *Water Res* 145:453–463. <https://doi.org/10.1016/J.WATRES.2018.08.055>
- Leichtweis J, Silvestri S, Carissimi E (2020) New composite of pecan nutshells biochar-ZnO for sequential removal of acid red 97 by adsorption and photocatalysis. *Biomass Bioenergy* 140:105648. <https://doi.org/10.1016/J.BIOMBIOE.2020.105648>
- Li Y, Wang J, Yao H et al (2011) Efficient decomposition of organic compounds and reaction mechanism with BiOI photocatalyst under visible light irradiation. *J Mol Catal A Chem* 334:116–122. <https://doi.org/10.1016/J.MOLCATA.2010.11.005>
- Lu L, Shan R, Shi Y et al (2019) A novel TiO₂/biochar composite catalysts for photocatalytic degradation of methyl orange. *Chemosphere* 222:391–398. <https://doi.org/10.1016/J.CHEMOSPHERE.2019.01.132>
- Makama AB, Salmiaton A, Choong TSY et al (2020) Influence of parameters and radical scavengers on the visible-light-induced degradation of ciprofloxacin in ZnO/SnS₂ nanocomposite suspension: identification of transformation products. *Chemosphere* 253:126689. <https://doi.org/10.1016/J.CHEMOSPHERE.2020.126689>
- Mirmasoomi SR, Mehdipour Ghazi M, Galedari M (2017) Photocatalytic degradation of diazinon under visible light using TiO₂/Fe₂O₃ nanocomposite synthesized by ultrasonic-assisted impregnation method. *Sep Purif Technol* 175:418–427. <https://doi.org/10.1016/J.SEPPUR.2016.11.021>
- Moawed EA, Eissa MS, Al-Tantawy SA (2022) Application of polyurethane foam/zinc oxide nanocomposite for antibacterial activity, detection, and removal of basic dyes from wastewater. *Int J Environ Sci Technol*. <https://doi.org/10.1007/s13762-022-04428-w>
- Mohammed RR, Chong MF (2014) Treatment and decolorization of biologically treated palm oil mill effluent (POME) using banana peel as novel biosorbent. *J Environ Manag* 132:237–249. <https://doi.org/10.1016/J.JENVMAN.2013.11.031>
- Monteagudo JM, Durán A, Martín IS, Vellón B (2020) Photocatalytic degradation of aniline by solar/TiO₂ system in the presence of the electron acceptors Na₂S₂O₈ and H₂O₂. *Sep Purif Technol* 238:116456. <https://doi.org/10.1016/J.SEPPUR.2019.116456>
- Munagapati VS, Yarramuthi V, Kim Y et al (2018) Removal of anionic dyes (reactive black 5 and congo red) from aqueous solutions using banana peel powder as an adsorbent. *Ecotoxicol Environ Saf* 148:601–607. <https://doi.org/10.1016/J.ECOENV.2017.10.075>
- Nippes RP, Macruz PD, Scaliante MHNO (2022) Enhanced photocatalytic performance under visible light of TiO₂ through incorporation with transition metals for degradation of 17 α -ethynylestradiol. *Int J Environ Sci Technol*. <https://doi.org/10.1007/s13762-022-04361-y>
- Palominos R, Freer J, Mondaca MA, Mansilla HD (2008) Evidence for hole participation during the photocatalytic oxidation of the antibiotic flumequine. *J Photochem Photobiol A Chem* 193:139–145. <https://doi.org/10.1016/J.JPHOTOCHEM.2007.06.017>
- Patel M, Kumar R, Pittman CU, Mohan D (2021) Ciprofloxacin and acetaminophen sorption onto banana peel biochars: environmental and process parameter influences. *Environ Res* 201:111218. <https://doi.org/10.1016/J.ENVRES.2021.111218>
- Picos-Benítez AR, Martínez-Vargas BL, Duron-Torres SM et al (2020) The use of artificial intelligence models in the prediction of optimum operational conditions for the treatment of dye wastewaters with similar structural characteristics. *Process Saf Environ Prot* 143:36–44. <https://doi.org/10.1016/J.PSEP.2020.06.020>
- Sakarkar S, Muthukumran S, Jegatheesan V (2020) Factors affecting the degradation of remazol turquoise blue (RTB) dye by titanium dioxide (TiO₂) entrapped photocatalytic membrane. *J Environ Manag* 272:111090. <https://doi.org/10.1016/J.JENVMAN.2020.111090>
- Samsami S, Mohamadi M, Sarrafzadeh MH et al (2020) Recent advances in the treatment of dye-containing wastewater from textile industries: overview and perspectives. *Process Saf Environ Prot* 143:138–163. <https://doi.org/10.1016/J.PSEP.2020.05.034>
- Santiago DE, Araña J, González-Díaz O et al (2014) Effect of inorganic ions on the photocatalytic treatment of agro-industrial wastewaters containing imazalil. *Appl Catal B Environ* 156–157:284–292. <https://doi.org/10.1016/J.APCATB.2014.03.022>
- Shfeizadeh S, Bayati B, Silva-Martínez S et al (2022) Experimental and modelling study of dye removal by photocatalysis with chitin-stabilized TiO₂/ZnO nanocomposite. *Int J Environ Sci Technol* 19:7321–7336. <https://doi.org/10.1007/s13762-021-03638-y>
- Sidik DAB, Hairom NHH, Ahmad MK et al (2020) Performance of membrane photocatalytic reactor incorporated with ZnO-Cymbopogon citratus in treating palm oil mill secondary effluent. *Process Saf Environ Prot* 143:273–284. <https://doi.org/10.1016/J.PSEP.2020.06.038>
- Silvestri S, Gonçalves MG, Da Silva Veiga PA et al (2019) TiO₂ supported on salvinia molesta biochar for heterogeneous photocatalytic degradation of acid orange 7 dye. *J Environ Chem Eng* 7:102879. <https://doi.org/10.1016/J.JECE.2019.102879>
- Singh J, Kumar V, Kim KH, Rawat M (2019) Biogenic synthesis of copper oxide nanoparticles using plant extract and its prodigious potential for photocatalytic degradation of dyes. *Environ Res* 177:108569. <https://doi.org/10.1016/J.ENVRES.2019.108569>



- Suresh M, Sivasamy A (2020) Fabrication of graphene nanosheets decorated by nitrogen-doped ZnO nanoparticles with enhanced visible photocatalytic activity for the degradation of methylene blue dye. *J Mol Liq* 317:114112. <https://doi.org/10.1016/J.MOL-LIQ.2020.114112>
- Tang T, Lu G, Wang W et al (2018) Photocatalytic removal of organic phosphate esters by TiO₂: effect of inorganic ions and humic acid. *Chemosphere* 206:26–32. <https://doi.org/10.1016/J.CHEMOSPHERE.2018.04.161>
- Thor SH, Ho LN, Ong SA et al (2020) Explicating the importance of aeration and pH for Amaranth degradation and electricity generation in a viable hybrid system of photocatalytic fuel cell and electro-fenton process. *Sep Purif Technol* 239:116535. <https://doi.org/10.1016/J.SEPPUR.2020.116535>
- Wang C, Zhu L, Wei M et al (2012) Photolytic reaction mechanism and impacts of coexisting substances on photodegradation of bisphenol A by Bi₂WO₆ in water. *Water Res* 46:845–853. <https://doi.org/10.1016/J.WATRES.2011.11.057>
- Wang N, Li X, Yang Y et al (2020) Photocatalytic degradation of sulfonamides by Bi₂O₃-TiO₂/PAC ternary composite: mechanism, degradation pathway. *J Water Process Eng* 36:101335. <https://doi.org/10.1016/J.JWPE.2020.101335>
- Xu W, Xu L, Pan H et al (2022) Superamphiphobic cotton fabric with photocatalysis and ultraviolet shielding property based on hierarchical ZnO/halloysite nanotubes hybrid particles. *Colloids Surfaces A Physicochem Eng Asp* 654:129995. <https://doi.org/10.1016/J.COLSURFA.2022.129995>
- Yoon JW, Baek MH, Hong JS et al (2012) Photocatalytic degradation of azo dye using TiO₂ supported on spherical activated carbon. *Korean J Chem Eng* 29:1722–1729. <https://doi.org/10.1007/s11814-012-0076-2>
- Zelmanov G, Semiat R (2015) The influence of competitive inorganic ions on phosphate removal from water by adsorption on iron (Fe+3) oxide/hydroxide nanoparticles-based agglomerates. *J Water Process Eng* 5:143–152. <https://doi.org/10.1016/J.JWPE.2014.06.008>

Springer Nature or its licensor (e.g. a society or other partner) holds exclusive rights to this article under a publishing agreement with the author(s) or other rightsholder(s); author self-archiving of the accepted manuscript version of this article is solely governed by the terms of such publishing agreement and applicable law.

